Experimental Mechanics (2014) 54:379–391
DOI 10.1007/s11340-013-9814-6

Residual Stress Measurement Using Hole Drilling and Integrated Digital Image Correlation Techniques

A. Baldi

Received: 29 May 2013 / Accepted: 23 September 2013 / Published online: 8 October 2013

Abstract The effectiveness of optical (mostly interferometric) methods for the measurement of residual stresses is largely demonstrated in literature. Nevertheless, these techniques are still confined to optical laboratories due to their high sensitivity to vibrations which makes it very difficult to perform the measurement in an industrial environment. Digital Image Correlation (DIC) has recently been proposed as a possible solution to this problem: this non-interferometric technique is much less affected by vibrations, but its sensitivity is relatively low, thus negatively affecting the accuracy of results.

This work proposes to use a variant of Digital Image Correlation, known as Integrated DIC (iDIC), in combination with the hole drilling technique. Since iDIC directly incorporates in its formulation the displacement field related to hole drilling, it overcomes most of the problems of standard DIC; in this way it is possible to obtain accurate results without using interferometric techniques.

Keywords Residual stress · Hole drilling · Integrated digital image correlation · Optical techniques

Introduction

The measurement of residual stress using the relaxation approach in combination with optical techniques has been proposed by several authors in past years. Indeed, optical experimental techniques (in particular interferometric ones) are well suited for residual stress measuring owing to several favorable characteristics: their high sensitivity (which can also be fine-tuned in some experimental techniques), the non-contact nature of the measurement and full-field data acquisition make them serious competitors of the standard strain-gauge-based procedure. Thus, several authors have proposed different approaches to residual stress measuring, mainly using holographic interferometry [1–4], grating (moiré) interferometry [5–8] and speckle interferometry [9–15]; orthotropic materials have also been considered [16, 17]. However, most of these approaches use the optical measuring technique as a direct replacement of strain gauges [2] or employ only few data points [3, 7, 8], thus not taking advantage of the availability of a huge number of sampling points that make it possible to use statistical approaches, i.e. it makes possible the exploitation of data redundancy to improve measurement accuracy and reliability [10, 11, 13, 18–21].

Even though the use of optical techniques is advantageous with respect to strain-gauges—they have similar, or higher sensitivity, they require little or no preprocessing of the area where the measurement is to be performed, they can be used in a wider range of temperatures—the use of these techniques is mainly confined to optical laboratories. Indeed, high sensitivity to vibrations makes the use of interferometric techniques very difficult in an industrial environment.

Digital Image Correlation is a non-interferometric technique able to measure bi- and three-dimensional displacement fields. It works by numerically correlating two images (two couples of images in the 3D case) acquired before and after motion under the assumption that pixel intensity remains constant during the acquisition. Since this approach

A. Baldi (✉)
Dipartimento di Ingegneria Meccanica,
Chimica e dei Materiali,
Università di Cagliari,
Piazza d'Armi, 09123 Cagliari, Italy
e-mail: antonio.baldi@dimcm.unica.it

results in an under-constrained set of equations (see next section), the solution is mostly obtained in the least square framework, thus each measurement corresponds to a local fit over a small (usually square) region, known as a *block*. The resulting algorithm is clearly nonlinear because the intensities at the inspected points (of the image to be compared) depend on the displacement components, thus a Newton-like algorithm (e.g. Levenberg-Marquardt) has to be used.

Although some authors have proposed the use of DIC for residual stress measurement [22–29], Digital Image Correlation is not the best optical technique to be coupled with hole drilling for residual stress measurement: indeed, due to the least square approach, the standard deviation of the measured displacement components depends on the square root of the number of points involved in the comparison; in presence of gradients (i.e. near the hole boundary, where most of the signal related to the drilling is located) the block must be small to enable the measurement to follow the fast variation of the signal. Thus the standard deviation of displacements is quite large; moreover the number of independent measurements (to be used by the reverse calibration algorithm to estimate residual stress) is relatively small when compared to interferometric techniques and each of them is somewhat biased [30] because the shape functions usually employed by standard codes are unable to correctly describe the residual-stress-related displacement field.

Better results can be obtained on moving from the "local" approach (i.e. using completely disjoined blocks) to a "global" DIC approach [31]. In this formulation, the displacement field is described using a mesh, thus involving a formalism identical to that used in the Finite Element field. The algorithm tries to optimize the displacement of nodes (which by themselves control the displacements inside the elements via the shape functions); thus minimization affects the full active area of the image (i.e. the region covered by elements) at the same time. In other words, since nodes are shared by adjacent elements, this approach results in a global minimization. Although the uncertainty of displacement is smaller when using the global formulation [32], the aforementioned problem regarding the number of pixels per block (element) is still present (even though it is less serious) thus making it difficult to follow large gradients in any case. Figure 1 shows the measured ϵ_{xx} field (selected because it better visualizes potential inhomogeneity) in an experimental hole drilling test. The analysis was performed using a global code; the results are generally correct, but a more detailed inspection shows that a) at a low residual stress level, a large part of the signal is located in a relatively small area, i.e. near the border of the hole (where the ements are smaller); b) it is possible to detect some errors near the border of the hole, thus confirming the previous discussion.

Integrated DIC (iDIC) was first proposed by Roux and Hild [33] and its first application to residual stress is the work of Gao and Shang [22]. It formally does not differ from a standard *local* DIC approach, but deserves a special acronym because of a single, but significant, modification: instead of using general-purpose shape functions to describe how the block of pixels moves and deforms, it uses problem-specific shape functions (i.e. the expected behavior of the problem to be studied is directly included in the formulation). This allows us to overcome the difficulties shown by all general-purpose codes in presence of large gradients: indeed, by integrating the expected behavior of the specimen inside the shape functions, the problem of biased measurements is completely sidestepped and there is no need for partitioning the domain into sub-regions, thus

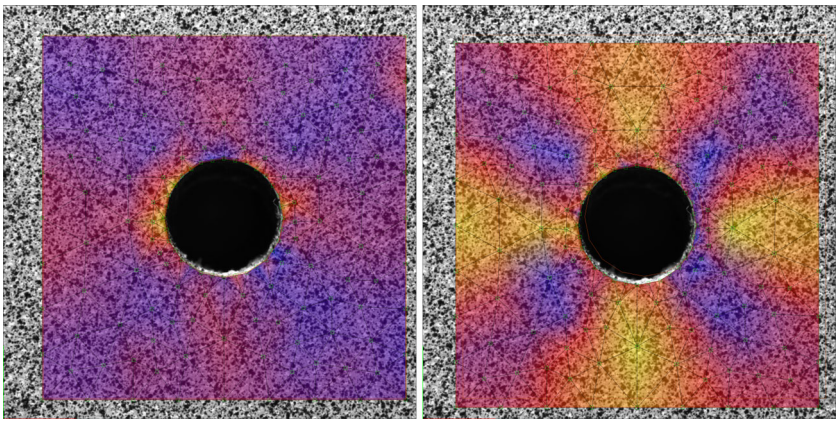

Fig. 1 Residual stress analysis using a global-DIC code; experimental data, ϵ_{xx} field (Material of specimen is AISI 304, thus Young's modulus is about 200 GPa, whereas hole diameter and thickness are respectively 4 and 5 mm). *Left*: $\sigma_y = 6$ MPa, *right*: $\sigma_y = 60$ MPa. Note the noise near the hole, clearly visible in the 6 MPa case, but detectable also in the 60 MPa case. Note also that even for a stress value as low as 6 MPa, the stress-related strain pattern can still be recognized

a huge number of pixels can be used for the analysis and the problem of the large standard deviation of displacements is completely solved. Moreover, the fitting algorithm directly involves the stress components related to residual stresses, thus allowing a direct measurement without any post-processing (i.e. the code is significantly simpler than coupling a standard DIC code with a-posteriori residual stress fitting).

This article is organized as follows: in the next section the general DIC formalism will be sketched and the modifications required to integrate the residual-stress-related displacement field in the formulation will be presented. Then the proposed formulation will be validated using numerical generated images (Section "Numerical Validation") and experimental tests (Section "Experimental Validation"). Section iDIC Vs Interferometric Analysis compares the performance of iDIC with respect to speckle interferometry, whereas some potential issues and the modification required to avoid them are discussed in Section "Discussion". Finally, Section "Conclusions" presents some conclusions.

i-DIC

The basic assumption of Digital Image Correlation is the constancy in time of the intensity of each point of the imaged object [34], i.e.

$$I(x, y, t) = I(x + u_x, y + u_y, t + \Delta t) \tag{1}$$

where $(x + u_x, y + u_y)$ is the location at time $t + \Delta t$ of the point which at time t was in (x, y). To satisfy this hypothesis, some constraints on the illumination and characteristics of the imaged surface have to be satisfied [35]—in short, the illumination should be isotropic and constant in time and the surface should present a non-periodic pattern—which can easily be fulfilled with careful design of the experimental setup.

Assuming the displacements to be small, the second member of equation (1) can be expanded in Taylor series truncated to the first order to obtain, after some easy mathematical manipulations, the well-known *optical flow* equation:

$$\frac{\partial I}{\partial x} V_x + \frac{\partial I}{\partial y} V_y + \frac{\partial I}{\partial t} = 0 \tag{2}$$

where V_x and V_y are the x and y components of velocity.

Equation (2) involves two unknowns, thus it is not possible to estimate the displacement field unless an auxiliary constraint is added to the formulation. Several solutions have been suggested to solve the so-called *aperture problem*, e.g. the local regularization constraint of Horn and Schunck [36], or the combined Local and Global approach of Bruhn et al. [37], but the most known approach to this problem is probably the Lucas and Kanade (LK) formulation [38], which minimizes, in the least square sense, an error function on patches of pixels under the assumption of an affine displacement model for the motion. The LK approach allows development of general-purpose codes either by following the displacement of each point independently (i.e. analyzing a block of pixels centered at the inspection point) or by writing a global function as previously described.

The most frequently used error functions are the Correlation

$$\chi^2_{CC}(i_0, j_0, u, v) = 1 - \frac{\sum_k \sum_l I(k,l)\, J(k+u_x, l+u_y)}{\sqrt{\sum_k \sum_l I^2(k,l)} \sqrt{\sum_k \sum_l J^2(k+u_x, l+u_y)}}$$

and the Least Square Difference

$$\chi^2_{LSD}(i_0, j_0, u_x, u_y) = \sum_k \sum_l [I(k,l) - J(k + u_x, l + u_y)]^2$$

where i_0 and j_0 are the coordinates of the pixel where the measurement is performed, u_x and u_y the X and Y displacement components to be measured, k and l range over the rows (columns) of the block centered at (i_0, j_0) (or over the pixel inside the mesh, in the global case) and finally I and J are the intensities of the reference and target images (i.e. the images of the specimen before and after motion).

To fit J to I, the error function has to be minimized; this involves estimating the derivatives of χ^2 with respect to the parameters that control the displacement (i.e. the parameters of the shape functions) and setting them to zero. The resulting solution system $\mathbf{Ax} = \mathbf{b}$ can easily be estimated, with $\mathbf{A} = \sum_i \mathbf{h}_i \mathbf{h}_i^{\mathrm{T}}$, the known terms vector $\mathbf{b} = \sum_i (I_i - J_i)\mathbf{h}_i$ and the vector $\mathbf{h}_i$ depending on the derivatives of the image intensity at the inspected points[1] i.

In the previously discussed formulation, the intensity of the test image was expanded in Taylor series. However, it is also possible to expand in series the intensity of the reference image I (or both [39]). The resulting algorithms converge to the same result, but are quite different from the implementation standpoint: indeed, since the reference image does not change in time, the latter solution allows somewhat faster execution of the iterative loop, because intensity derivatives can be evaluated before entering the main body of the procedure. However, the improvement is not so significant because a) the most computationally intensive step of the algorithm is the intensity interpolation, which has to be performed in any case; b) the total

[1] To simplify notation, a single index was used to address pixel coordinates. This is not a problem providing that we select a row/column ordering, e.g. $i = kw + l$ (row-major order), or $i = k + hl$ (column-major order), where k and l are the row and column indexes and w and h are the width and height of the image.

number of iterations is somewhat larger due to the constant derivatives.

Note that the solution system appears to be linear, but this is not the case. Indeed, both J and its derivatives with respect to the x and y axes appearing in $\mathbf{h}_i$ depend on the unknown displacements (which control where these quantities must be evaluated); thus, to achieve a solution, a nonlinear iterative approach is required.

As previously noted, general-purpose codes use linear (sometimes parabolic) shape functions [34]:

$$u_x = p_0 + (1+p_1)\xi + p_2\eta + \left[p_3\xi^2 + p_4\xi\eta + p_5\eta^2\right] \quad (3)$$

$$u_y = q_0 + q_1\xi + (1+q_2)\eta + \left[q_3\eta^2 + q_4\xi\eta + q_5\xi^2\right] \quad (4)$$

where ξ and η are the coordinates of a local system with the origin at (i_0, j_0) and the p_i and q_i are the unknown parameters; thus, the mapping can be assumed to correctly follow the real behavior only locally and several fits (elements) have to be performed to describe complex fields. This is not the case in iDIC: since it targets a well-defined problem, specific shape functions can be used to describe the displacement field globally. Thus, there is no need to perform several local measurements and a truly-global solution is obtained.

To convert the above-sketched general framework to an iDIC approach, we have to replace the generic displacement functions with residual-stress specific shape functions; in fact, the displacement field induced around a hole by residual stress relaxation is well known:

$$u_r = A\left(\sigma_x + \sigma_y\right) + B\left[\left(\sigma_x - \sigma_y\right)\cos(2\theta) + 2\tau_{xy}\sin(2\theta)\right] \quad (4a)$$

$$u_\theta = C\left[\left(\sigma_x - \sigma_y\right)\sin(2\theta) - \tau_{xy}\cos(2\theta)\right] \quad (4b)$$

$$u_z = F\left(\sigma_x + \sigma_y\right) + G\left[\left(\sigma_x - \sigma_y\right)\cos(2\theta) + 2\tau_{xy}\sin(2\theta)\right] \quad (4c)$$

where the A, B, C, F and G coefficients can be estimated using Finite Element computations [10], or from the theoretical solution given by Nelson et al. [3]:

$$A = \frac{r_0}{2E}(1+\nu)\rho \qquad B = \frac{r_0}{2E}\left[4\rho - (1+\nu)\rho^3\right]$$
$$C = -\frac{r_0}{2E}\left[2(1-\nu)\rho + (1+\nu)\rho^3\right] \qquad F = 0$$
$$G = \frac{\nu t}{E}\rho^2 \quad (5)$$

where ρ is the ratio of the hole radius r_0 and the distance of the current point from the center of the hole ($0 \leq \rho \leq 1$), E is the Young modulus, ν the Poisson ratio, t the thickness of the plate, r, θ and z the coordinate of the point in a cylindrical reference system and σ_x, σ_y and τ_{xy} the (orthogonal) stress components.

The in-plane displacement components (equations (4a) and (4b)) can easily be projected in the x and y directions using a standard rotation matrix to finally obtain the sought for shape functions:

$$u_x(x, y, \sigma_x, \sigma_y, \tau_{xy}) = u_0 + P_u\sigma_x + Q_u\sigma_y + R_u\tau_{xy} \quad (6a)$$

$$u_y(x, y, \sigma_x, \sigma_y, \tau_{xy}) = v_0 + P_v\sigma_x + Q_v\sigma_y + R_v\tau_{xy} \quad (6b)$$

where P_u, Q_u and R_u (P_v, Q_v and R_v) are calibration coefficients depending on point location, material properties and hole geometry:

$$\begin{aligned} P_u &= [A + (B+C)\cos(2\theta) - C]\cos(\theta) \\ Q_u &= [A - B\cos(2\theta)]\cos(\theta) + C\sin(2\theta)\sin(\theta) \\ R_u &= +2[(B+C)\cos(2\theta) + B]\sin(\theta) \\ P_v &= [A + (B+C)\cos(2\theta) + C]\sin(\theta) \\ Q_v &= [A - (B+C)\cos(2\theta) - C]\sin(\theta) \\ R_v &= -2[(B+C)\cos(2\theta) - B]\cos(\theta) \end{aligned} \quad (7)$$

Note that equations (6a) and (6b) include two parameters (respectively u_0 and v_0) to account for rigid body motion of the specimen during testing.

Once the shape functions (6) are known, the development of the algorithm exactly follows the standard LK formulation; the *normal equation* solution matrix and the known-terms vector can be estimated as explained above, providing we write

$$\mathbf{h}_i = \begin{Bmatrix} \dfrac{\partial J_i}{\partial \xi} \\ \dfrac{\partial J_i}{\partial \eta} \\ P_u\dfrac{\partial J_i}{\partial \xi} + P_v\dfrac{\partial J_i}{\partial \eta} \\ Q_u\dfrac{\partial J_i}{\partial \xi} + Q_v\dfrac{\partial J_i}{\partial \eta} \\ R_u\dfrac{\partial J_i}{\partial \xi} + R_v\dfrac{\partial J_i}{\partial \eta} \end{Bmatrix} \quad (8)$$

where, similarly to equation (3), ξ and η are local variables in the reference system located in the reference image ($d\xi = dx$, $d\eta = dy$) and we have omitted the dependency of the calibration coefficients $P_u, \ldots, R_v$ on point i.

Validation

Validating a residual stress measurement algorithm is not easy. It would require performing the measurement on a specimen with known residual stresses (i.e. knowing the complete history of its technological treatments). Thus I opted for a two-step approach, first using numerically generated images, then performing a semi-experimental validation, i.e. an experimental campaign employing externally applied loads after residual stress relaxation.

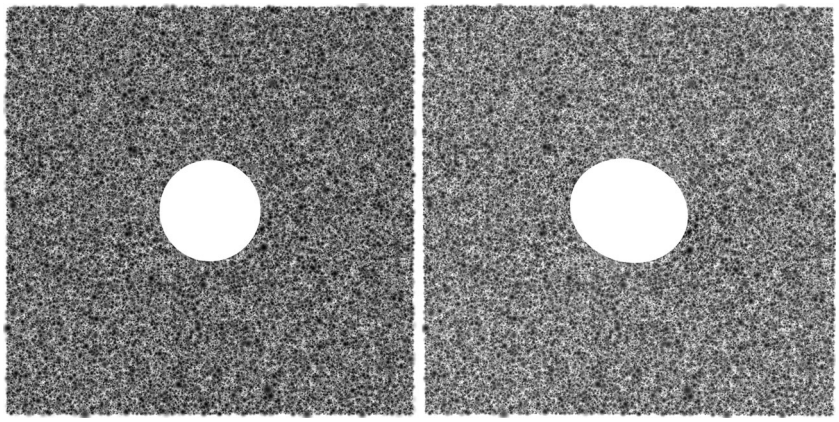

Fig. 2 Example of a simulated speckle field. *Left*: undeformed speckle field; *right*: after stress relaxation. To make the stress-induced displacement field apparent, unrealistic material parameters were used for the generation. ($\sigma_x = 100$ MPa, $\sigma_y = 50$ MPa, $\tau_{xy} = 20$ MPa, $E = 1000$ MPa, $\nu = 0.3$. Pixel size: 8 μm)

Numerical Validation

It is well known [40, 41] that generating images for DIC testing is not easy due to the sensitivity of the algorithm to errors induced by polynomial interpolation. To solve this problem I followed an analytical approach: the speckle field was described as the summation of several bell-shaped functions, randomly "sprayed" on the surface:

$$B(r) = \begin{cases} s\left[1 - (r/a)^2\right]^3 & r \le a \\ 0 & \text{elsewhere} \end{cases} \tag{9}$$

where a is the radius of the speckle, s is a scale factor ($0 < s \le 1$) and r is the radius from the center of the blob. Consequently, the intensity distribution is a continuous, known, analytical function resulting from the summation of all the B functions. Generating an image requires sampling the field on a grid of points and mapping (through the residual stress displacement field) the estimated intensities to the destination image [42]. This procedure is highly computation-intensive because each pixel has to be supersampled; moreover, each intensity estimation requires determining the list of the bell-shaped functions involved in the computation. However, by construction this procedure does not introduce any distortion in the speckle field. Figure 2 shows an example of the generated images before and after stress relaxation. To make the tress-induced displacement field apparent,[2] unrealistic parameters were used (in particular the Young modulus is about two orders of magnitude smaller than the typical values for metals). By examining specific speckle patterns it is quite easy to detect how the specimen deforms under loading.

Figure 3 shows the results of the validation analysis (performed using steel-compatible parameters: $E = 208$ GPa, $\nu = 0.3$): a monoaxial ($\sigma_1 = 200$ MPa) stress field was rotated using ten-degree steps starting from 0 up to 90°. After analyzing each of the synthesized images with the proposed algorithm, results were graphed as a function of the loading angle. The figure clearly shows the accuracy of the proposed algorithm: indeed, the estimated stress components (the square, circular and triangular markers, used respectively for σ_x, σ_y and τ_{xy}) exactly follow the theoretical behavior (the continuous line), the errors being smaller than 1 MPa. It should be noted that the algorithm is robust against noise: to simulate realistic data, the lower three bits of the image data were perturbed by adding uniform white noise, but the large number of pixels involved in the computation (∼

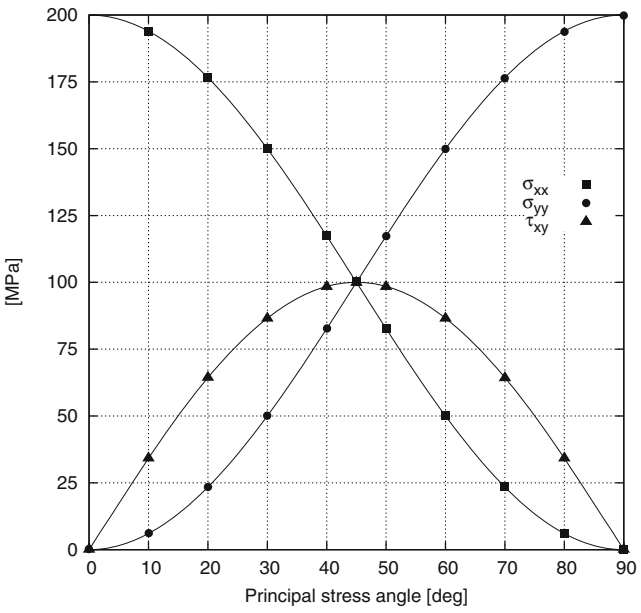

Fig. 3 iDIC reliability test (synthetic images). Applied stress is always the same (200 MPa), but using a different orientation (from 0 to $\pi/2$ by $\pi/18$ (10°) steps)

[2]The maximum displacement of the set of images used in the validation is about one pixel, which makes it impossible to detect the differences by the naked eye.

3 MPixel) makes the algorithm apparently insensitive to this perturbation.

Figure 4 confirms the robustness of the iDIC approach: a set of monodimensional residual stress images were synthesized starting from 10 up to 800 MPa (Young's modulus: 70 GPa, Poisson's ratio: 0.3, hole radius: 3 mm, quantization: 12 bit); on observing Fig. 4, it is apparent that iDIC was able to reliably estimate the residual stress with very small deviations from the theoretical value. As a comparison, Fig. 5 graphs the absolute errors in residual stress estimation for iDIC and for the standard approach (i.e. residual stresses are estimated by reverse calibration using as input either the u or v displacement field estimated by a standard DIC code). Even though errors are very small for both approaches, iDIC is significantly more accurate; moreover, the error range is clearly correlated with stress level in the standard approach, while it remains stable in the iDIC case. Note that the noiseless version of the images was used during error estimation, thus Fig. 5 may be viewed as a lower limit of the errors one should expect during a residual stress test.

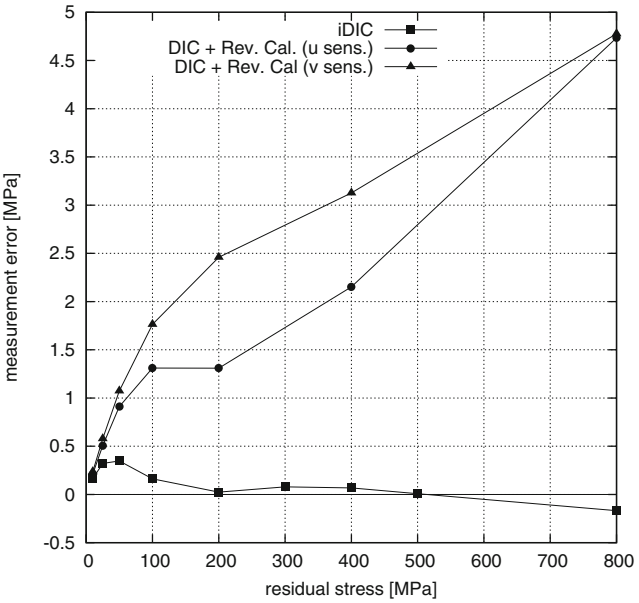

Fig. 5 Absolute errors in residual stress estimation using iDIC and the standard approach (i.e. general purpose DIC analysis coupled with a-posteriori reverse calibration). The noiseless version of the set of images used for Fig. 4 was employed

Experimental Validation

As previously noted, experimental validation requires knowing the expected residual stress values. To this end it is necessary to completely remove (e.g. by annealing) all stresses eventually induced during the manufacturing of the specimen and artificially inject known ones. Both points are somewhat critical because the former may alter the metallurgical characteristics of the material (e.g. its grain, the orientation of the fibers), whereas the latter requires accurately loading the specimen above the yield point, taking into account work hardening and potential instabilities. Thus, the induced stress values are usually not so accurate as we would like them to be. An alternate approach, able to better control the induced stress level, can be obtained by locally relaxing the specimen by material removal. The full procedure can be summarized in the following steps:

1. drill the hole in the specimen; in this way the residual stresses eventually present are released;
2. acquire the reference image;
3. apply a known stress state (either by using a load cell or with strain gauges glued to the specimen far from the hole);
4. acquire the new image (note that differently from the previously discussed procedure we are working in the elastic range);
5. perform the analysis.

This procedure is clearly erroneous because it corresponds to a tensile test of a plane with a hole. However, there exists a close relation between the residual stress field around a hole and the corresponding distribution on an infinite plate with a hole under tension: in fact, it is possible to obtain one

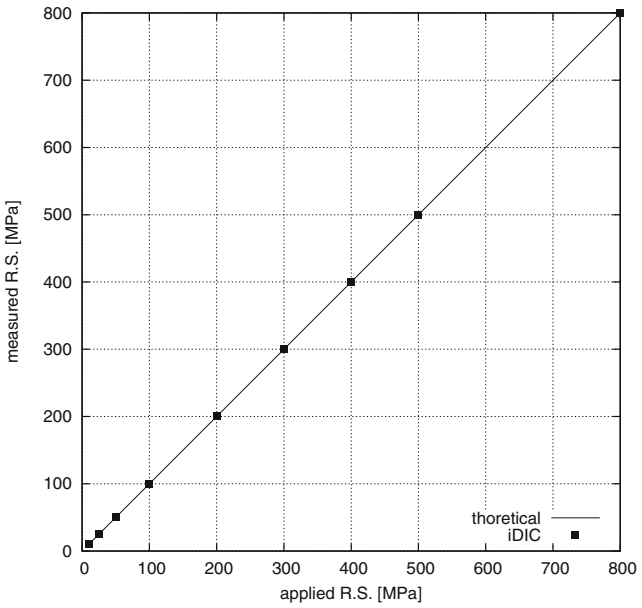

Fig. 4 iDIC range test: estimated residual stress Vs theoretical values (Synthetic images). Material parameters: $E = 70$ GPa, $\nu = 0.3$. Note that the iDIC code is able to measure from tiny to very large residual stresses with high accuracy (no modification of the software or acquisition settings was performed during the analyses)

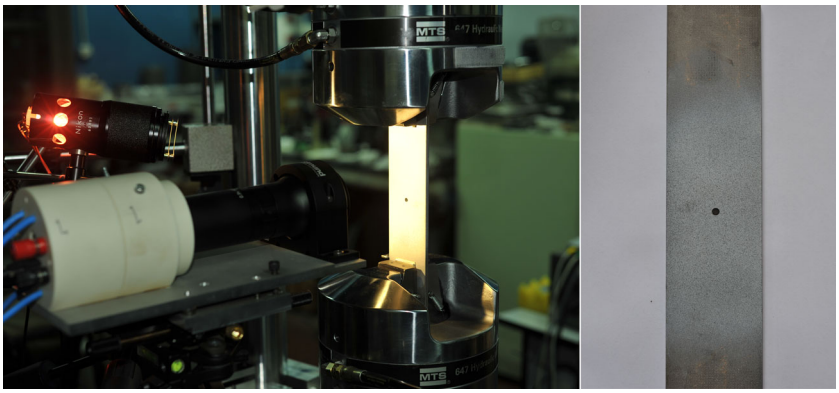

Fig. 6 Image of the specimen used for validating the iDIC code using tensile induced "residual stresses". *Left*: experimental setup; *right*: specimen

from the other by summing (subtracting) the displacement field of an infinite plane in tension:

$$u_x^p = \frac{\sigma_x - \nu\sigma_y}{E}x + \frac{\tau_{xy}}{2G}y$$
$$u_y^p = \frac{\tau_{xy}}{2G}x + \frac{\sigma_y - \nu\sigma_x}{E}y \tag{10}$$

Thus, the problem appears to be solved and the test can be performed. The proposed procedure has been used in various works (e.g. Baldi [43], Valentini et al. [16]); in particular, it gently fits for all interferometric approaches because the removal of the always present spurious drift, usually performed by least square fitting a plane to the phase field, automatically removes the displacement field (equation (10)). This is not really the case in the proposed iDIC approach: since the displacement field is never explicitly computed (we are directly fitting the stress components) there is no way to subtract a-posteriori the spurious displacement field (equation (10)). The only solution for obtaining a working algorithm is by including the appropriate correction factors in the shape function formulation; following this approach the various calibration coefficients become

$$P'_u = P_u + \frac{x}{E}Q'_u = Q_u - \frac{\nu x}{E}R'_u = R_u + \frac{y}{2G}$$
$$P'_v = P_v - \frac{\nu y}{E}Q'_v = Q_v + \frac{y}{E}R'_v = R_v + \frac{x}{2G} \tag{11}$$

where the prime flags the corrected coefficients.

Figure 6 shows the specimen used to perform experimental validation of our code: a 4 mm hole was drilled in an AISI 304 plate (section: 60 × 5 mm). Then the surface was painted to obtain a random speckle pattern. The specimen was installed in our testing machine (MTS Landmark 370) and loaded from 0 to 30 kN using 3 kN steps. It should be noted that each loading step can be viewed as a completely independent test since each image (acquired after loading) was processed against the unloaded case without any information from the previous analyses. Figure 7 shows the results of the numerical processing, the square markers being iDIC estimates, while the continuous line corresponds to the theoretical value. It is apparent that the iDIC-based code was able to correctly estimate the stress values even for very low loading levels.[3] The result is even more remarkable when considering that no previous mechanical characterization was performed on the specimen, thus both the Young modulus and Poisson coefficients are approximate values ($E = 200$ GPa, $\nu = 0.3$).

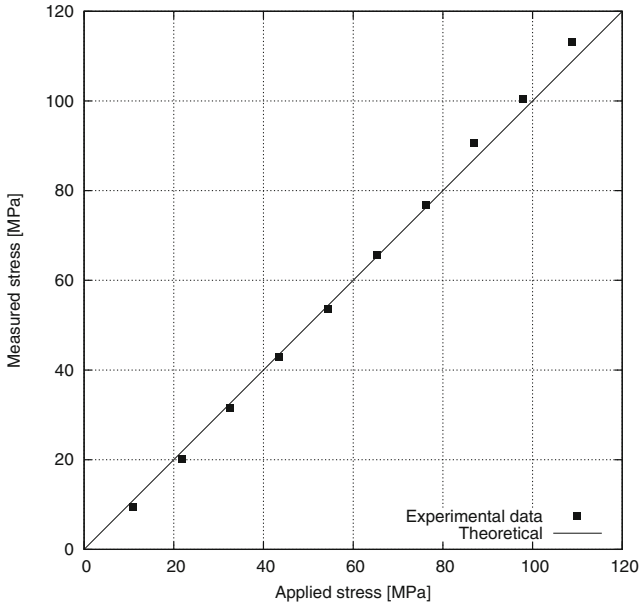

Fig. 7 Estimated residual stress Vs theoretical values (experimental data). Note that above 60 MPa (stress at infinity) plasticity starts to affect results (Yield stress of AISI 304 is 215 MPa at 0.2 % offset)

[3]Note that AISI 304 yields at 215 MPa, thus the deviation from linearity above 60 MPa visible in the graph is due to plasticity starting to affect the displacement field.

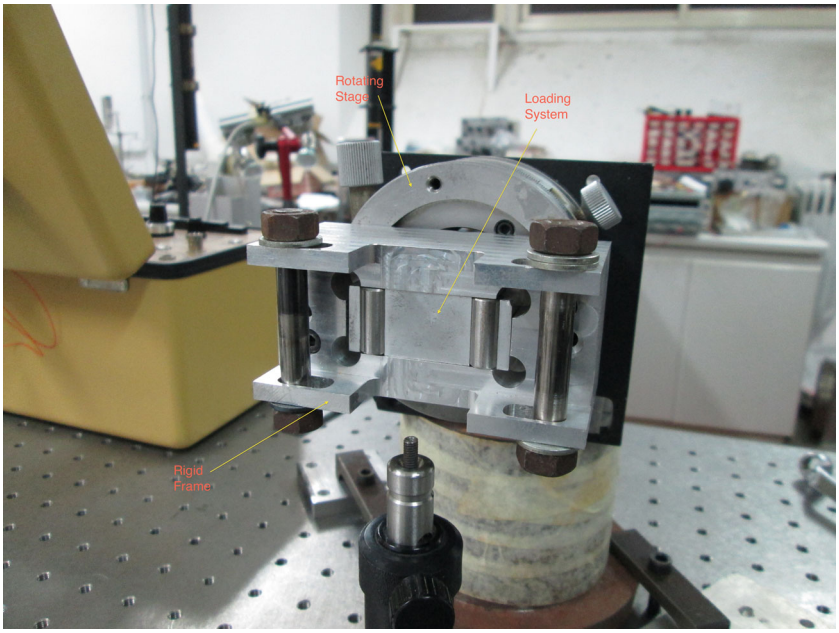

Fig. 8 Four-point-bending loading system

iDIC Vs Interferometric Analysis

To asses the accuracy of the proposed methodology, some experimental tests using both interferometric methods (in-plane and out-of-plane ESPI) and integrated Digital Image Correlation were performed. Because of the vibrations induced by the hydraulic system, it is not possible to use the servo-hydraulic testing machine employed in the previous section. Thus I opted for the four-point-bending system shown in Fig. 8: the loading frame is coupled to the micrometric loading screw by means of a spherical joint, thus (small) misalignments of the specimen will be automatically compensated; moreover, the fixed frame is mounted on a optical class rotating stage to allow alignment of the specimen with the plane of the optical beams; finally, the applied load is monitored by an in-house-built load cell (not visible in the image) mounted between the fixed frame and the loading screw.

Figure 9 (left) shows the acquired phase modulo 2π field using an in-plane-sensitive ESPI setup. The optical configuration is a standard Leendertz configuration (dual-illumination-, single-observation-direction method [44]) using a (symmetrical) illumination angle of about 18 degrees. A strain gauge was glued to the back side of the specimen to directly measure the stress level in the central area. The four-point bending configuration ensures a constant stress state in the region between the inner constraint, thus the above-described correction (equation (10)) applies. Figure 9 (right) shows the phase field after removal of the linear displacement component (note that the phase-unwrapped data were re-wrapped to simplify comparison). Although a low sensitivity configuration was used, I had to low-pass-filter the raw data to allow the unwrapping algorithm to work correctly due to the incipient decorrelation at the boundaries; thus the upper limit of the measuring range of the experimental technique is quite near the current stress value (100 MPa).[4]

Figure 10 (left) shows the wrapped phase field related to an out-of-plane ESPI experiment. The data analysis, apart from the higher quality of the fringes due to the smooth reference used in this optical configuration, shows an experimental problem not easily detectable in the previous experiment: indeed, even though the specimen is relatively thick,[5] it behaves like a plate, as is highlighted by the anticlastic shape it assumes under bending (see Fig. 11). The stress concentration factor around a hole of a plate in bending depends on the ratio of the hole radius to the plate thickness with an asymptotic value of about 1.8 (assuming $\nu = 1/3$) [45]. This means that

– the displacement field around the hole is significantly different from the assumed plane-strain model; this is particularly significant in the orthogonal direction with respect to the bending plane (the regions around the

[4]It should be noted that decorrelation is induced by both the large in-plane motion and by large rotation of the normal to surface caused by the externally applied bending load. No decorrelation occurs in the area near the hole, thus the measurement range of a true residual stress measurement is significantly larger.

[5]To reduce decorrelation problems in the in-plane ESPI test the specimen was made of steel (high Young's modulus) and is relatively thick (section is 25 × 3 mm).

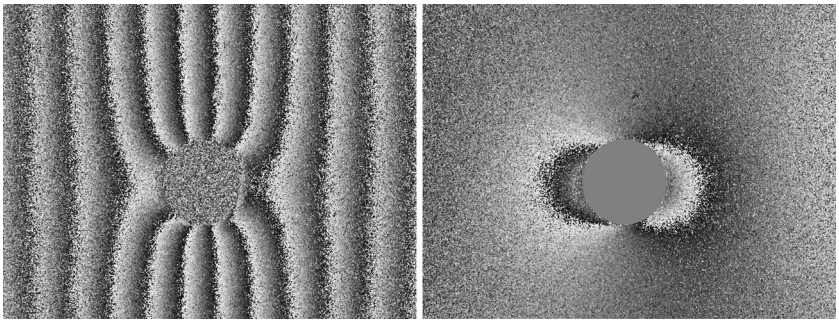

Fig. 9 Residual stress measurement using in-plane sensitive ESPI. *Left*: acquired phase modulo 2π field; *right*: the same data after removal of the interpolating plane

top and bottom of the hole in our case). Since σ_y (in current loading configuration) is mainly affected by displacements in these areas, its value will be incorrectly identified by both the interferometric and the digital correlation methods;

– the linear correction described in the previous section takes into account in-plane motion; the out-of-plane component compensation requires using a parabolic term both in the vertical and horizontal directions.

Figure 10 (right) shows the re-wrapped phase field after correction: a fast review of literature [3, 20, 21] shows that it is qualitatively correct even though it is affected by the aforementioned problem.

Figure 12 compares the σ_x measurements when estimated using iDIC, in-plane ESPI and out-of-plane ESPI: all three experimental approaches are very accurate, the largest error being about 2 MPa. iDIC errors are generally better than those of out-of-plane ESPI and comparable with those of in-plane ESPI. It should be noted that if comparison is performed on the σ_y, errors are very large due to the problem discussed above: in-plane ESPI is the most affected optical configuration because it estimates the influence of σ_y indirectly (through the effect of transversal contraction on X displacements); out-of-plane ESPI benefits from its mixed (in-plane and out-of-plane) sensitivity; finally, iDIC is significantly less erroneous, probably because it fits both X and Y displacements.

Discussion

The numerical and experimental validations of the previous section show that the proposed iDIC approach allows measurement of residual stress values with high reliability and accuracy. However, some details must be pointed out:

– From a practical viewpoint, the proposed experimental procedure cannot be performed as described. In fact, the calibration coefficients (equation (7)) depend on the relative position of the point where the coefficients $P_u \ldots R_v$ are estimated with respect to the center of the hole. Although in the previously described validation the specimen was drilled before acquisition of the reference image, in a true residual stress measurement the hole is drilled after acquisition of the reference image, thus it is not possible to correctly locate the center of the hole in the reference image. However, the problem can easily be solved by swapping the role of the reference and test images: in this case the hole exists, thus center and radius are known and the calibration coefficients can be estimated. The previously described procedure can be performed with no modification, except for a post -processing step for reversing the sign of the resulting residual stresses.

– As previously noted, DIC codes use a Newton-like iterative procedure to estimate displacements. This class of algorithms requires a starting point, which should

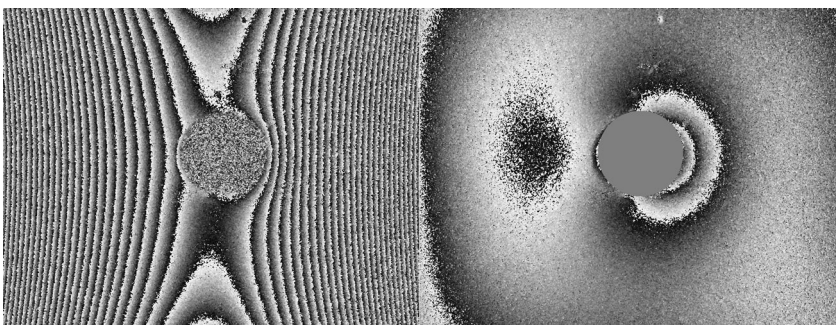

Fig. 10 Residual stress measurement using out-of-plane sensitive ESPI. *Left*: acquired phase modulo 2π field; *right*: the same data after removal of the anticlastic displacement field (Illumination angle: $\sim 63.5°$)

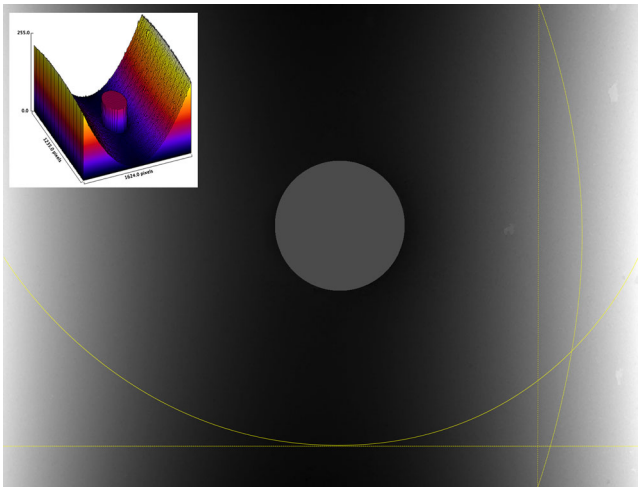

Fig. 11 Residual stress measurement using out-of-plane sensitive ESPI: unwrapped phase field. Taking into account that the sensitivity vector is mostly in the out-of-plane direction, it is apparent that the specimen undergoes an anticlastic deformation under bending, i.e. it behaves like a plate. Note the small unwrapping errors at the *right* boundary of the image

be near enough to the one sought; thus a simpler, less accurate, pre-processing step is usually executed using a matching-block algorithm (without taking into account deformations) or by the digital equivalent of speckle photography (FFT algorithm).[6] However, several empirical tests performed on synthetic images with random stress fields showed that this is not the case with the proposed iDIC algorithm, providing that rigid body motion has been correctly estimated. Indeed, even for a residual stress value as large as 800 MPa, the iDIC code converges to the correct value starting from $\sigma_x = 0$, $\sigma_y = 0$, $\tau_{xy} = 0$ (see Fig. 4). Thus, no preliminary estimate is required for the stress values. On the contrary, a modest error in the rigid body displacements makes it difficult to obtain convergence to the correct values. The solution to this problem is a pre-processing step to measure rigid body motion: actually the simple estimation of the displacements of the four corners of the active area, performed using a matching-block algorithm (without taking into account deformations), suffices to provide an estimate accurate enough to achieve convergence. Note that both the complexity and computational loads added by this pre-processing step are completely negligible.

– The proposed algorithm is potentially usable in an industrial environment (it needs only portable instrumentation that allows repositioning of the camera and/or drilling system). If this is the case, it is quite probable that the previously summarized requirements regarding specimen illumination will not be fulfilled. A partial solution can be obtained by including a global scale factor and a global offset of the intensities in the error functional [46]. Using this approach, the sum of the square differences error function becomes

$$\chi^2_{LSD} = \sum_k \sum_l \left\{ [\alpha I(k,l) + \beta] - J(k + u_x, l + u_y) \right\}^2$$

where α scales the intensities of the reference image and β adds a global offset. Using this approach, both images are modified: the intensities of reference image I are (globally) scaled and shifted respectively by α and β, whereas the test image J is moved and deformed by the displacement field. From a formal viewpoint, the solution system gains two rows and two columns (it becomes a 7×7 square matrix); indeed, assuming the rows (and columns) related to α and β to be respectively the first and second, $\mathbf{h}_i$ becomes:

$$\mathbf{h}_i = \begin{Bmatrix} -I_i \\ -1 \\ \frac{\partial J_i}{\partial \xi} \\ \frac{\partial J_i}{\partial \eta} \\ P_u \frac{\partial J_i}{\partial \xi} + P_v \frac{\partial J_i}{\partial \eta} \\ Q_u \frac{\partial J_i}{\partial \xi} + Q_v \frac{\partial J_i}{\partial \eta} \\ R_u \frac{\partial J_i}{\partial \xi} + R_v \frac{\partial J_i}{\partial \eta} \end{Bmatrix} \tag{12}$$

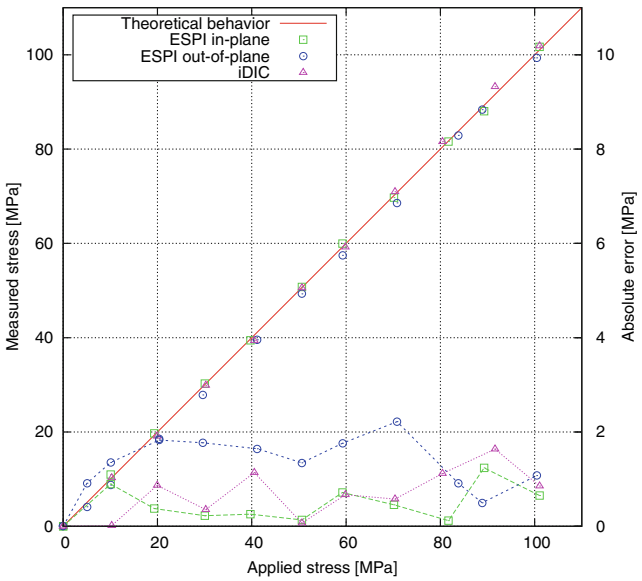

Fig. 12 ESPI Vs iDIC: accuracy comparison. Results of the iDIC method are comparable to those of the interferometric methods. Note that absolute errors are very low for all three experimental methodologies, the largest error being about 2 MPa for the out-of-plane ESPI at 70 MPa (Note that the scale used to plot errors is ten times larger than the one used for stress values)

[6] An alternate solution uses a pyramidal approach, i.e. the reference and test images are repeatedly compressed using a Laplacian filter to construct two pyramids of images. An optical flow analysis is executed for each level of the image stack, using the previous estimate as the starting point of the successive, more accurate, computation.

whereas $\mathbf{b} = -\sum_i J_i \mathbf{h}_i$.

- The formulation can be further refined by taking into account the rigid body rotation ω around the center of the hole (i.e. by writing $\mathbf{u} = \mathbf{u_0} + \omega \times \mathbf{r}$). With this approach, the shape functions (equation 6) become:

$$u_x = u_0 - \omega\eta + P_u\sigma_x + Q_u\sigma_y + R_u\tau_{xy} \tag{13a}$$

$$u_y = v_0 + \omega\xi + P_v\sigma_x + Q_v\sigma_y + R_v\tau_{xy} \tag{13b}$$

and the new term (related to the ω degree of freedom)

$$\frac{\partial J_i}{\partial \xi}\eta + \frac{\partial J_i}{\partial \eta}\xi \tag{14}$$

has to be inserted in the $\mathbf{h}_i$ vector given above (equation (12); note that the ξ and η coordinates appearing in equation (14) must be related to a local reference system with the origin located at the center of the hole). However, the estimated ω was very small in all tests that we performed and no significant variation of the results was observed, thus the inclusion of the rigid-body-rotation degree of freedom in the formulation is not strictly required.

- It is well known that polynomial interpolation significantly affects the accuracy of DIC codes [40, 47–49]. This is also the case with the proposed formulation, with a significant difference: all the related articles in literature flag the B-Spline cubic approximant as the best cubic polynomial. Actually, an empirical comparison performed employing some of the most commonly used polynomials[7] shows that between the cubic polynomial the best accuracy is obtained by the Lagrangian interpolant; moreover, using a quintic polynomial provides no significant improvement.
- Throughout this article reference has consistently been made to the theoretical coefficients related to the hole through case (equation (5)); however, this is in no way required by the proposed approach: it is well known that in the blind-hole case the displacement field can still be written using equations (4a)–(4c), provided we use a set of $A \ldots G$ coefficients related to the specific hole geometry: using Finite-Element-estimated calibration coefficients [50, 51], iDIC is able to measure residual stress in the blind hole configuration (and give the correct estimate for σ_y in the previously discussed cases).
- Although it has not been discussed, it is quite easy to formulate the iDIC algorithm (equations (6a)–(7)) in terms of $P = (\sigma_x + \sigma_y)$, $Q = (\sigma_x - \sigma_y)$ and τ_{xy}. However, empirical tests show no significant difference between the two approaches: results of the two formulations agree within the limit of the numerical tolerance used in the iterative loop.

[7] Bilinear, cubic interpolant, cubic and quintic Lagrangian interpolant, cubic and quintic B-spline approximant.

Conclusions

In this work an integrated DIC approach for residual stress measurement is analyzed. The hole-drilling-related displacement field is well known, thus it is possible to replace the standard shape functions of the block with specific functions, obviously augmented by a rigid translation component and (optionally) illumination parameters and rigid body rotation to account for rigid body motion during drilling and potential drift of the illumination. Sampling of multiple locations to follow the data is no longer required and the full image constitutes a single patch whose deformation is controlled by five (eight) parameters: the three residual stress components, the two in-plane rigid translations and optionally the intensity compensation coefficients and rigid body rotation. Since the uncertainty of the method directly depends on the number of pixels involved in evaluation of the error function, this approach results as being quite effective and allows replacement of interferometric techniques with Digital Image Correlation. The advantages are significant: DIC does not require coherent illumination and is much more robust against vibrations, thus making possible the use of optical methods in industrial environments. Computation time is very short: a complete analysis of a 2048×2048 image requires only a few seconds, a large fraction of which is required to pre-compute the calibration coefficients.

A final note: it is worth noting that DIC sensitivity is always measured in pixels and is always the same (about 1/100 of a pixel) irrespective of the real pixel size. This is completely different from the case of interferometric techniques, where sensitivity is mainly controlled by the wavelength of the light source. From a practical viewpoint this means that it is possible to tune sensitivity by selecting the magnification of the telecentric lens and vice versa (i.e. it is possible to adjust the hole diameter to the optic); moreover, it is possible to perform measurements also at microscale, providing there is a suitable imaging system and a random speckle pattern.

References

1. Lin ST, Hsieh CT, Lee CK (1995) Full field phase-shifting holographic blind-hole techniques for in-plane residual stress detection. In: Honda T (ed) International conference on applications of optical holography, vol 2577. Proceedings of SPIE, Bellingham, pp 226–237

2. Nelson DV, McCrickerd JT (1986) Residual-stress determination through combined use of holographic interferometry and blind hole drilling. Exp Mech 26:371–378
3. Nelson DV, Makino A, Fuchs EA (1997) The holographic-hole drilling method for residual stress determination. Optics Lasers Eng 27:3–23
4. Steinzig M, Hayman G, Rangaswamy P (2001) Data reduction methods for digital holographic residual stress measurement. In Proceedings of the SEM annual conference and exposition on experimental and applied mechanics, Portland, OR, p 2001
5. Bulhak J, Lu J, Montay G, Surrel Y, Vautrin A (2000) Grating shearography and its application to residual stress evaluation. In: Jacquot P, Fournier JM (eds) Interferometry in speckle light: theory and applications. Springer, Berlin, pp 607–614
6. Schwarz RC, Kutt LM, Papazian JM (2000) Measurement of residual stress using interferometric Moiré: a new insight. Exp Mech 40(3):271–281
7. Wu Z, Lu J (2000) Study of surface residual stress by three-dimensional displacement data at a single point in hole drilling method. J Eng Mater Technol 122(2):215–220
8. Wu Z, Lu J, Han B (1998) Study of residual stress distribution by a combined method of Moiré interferometry and incremental hole drilling, Part I: theory. J Appl Mech 65(4):837–843
9. Albertazzi AJ, Kanda C, Borges MR, Hrebabetzky F (2000) A radial in-plane interferometer for espi measurement. In: Kujawinska M, Pryputniewicz RJ, Takeda M (eds) Laser interferometry X: techniques and analysis, vol 4101. Proceedings of SPIE, Bellingham, pp 77–88
10. Baldi A (2005) A new analytical approach for hole drilling residual stress analysis by full field method. J Eng Mater Technol 127(2):165–169
11. Baldi A, Jacquot P (2003) Residual stresses investigations in composite samples by speckle interferometry and specimen repositioning. In: Gastinger K, Løkberg OJ, Winther S (eds) Speckle metrology 2003. Proceedings of SPIE, Bellingham, Washington vol 4933, pp 141–148
12. Diaz FV, Kaufmann GH, Galizzi GE (2000) Determination of residual stresses using hole drilling and digital speckle pattern interferometry with automated data analysis. Opt Lasers Eng 33(1):39–48
13. Focht G, Schiffner K (2002) Numerical processing of measured full-field displacement data around holes for residual stress determination. In: Mang HA, Rammerstorfer FG, Eberhrdsteiner J (eds) Fifth world congress on computational mechanics, Vienna Austria
14. Vikram CS, Pechersky MJ, Feng C, Engelhaupt D (1996) Residual-stress analysis by local laser heating and speckle-correlation interferometry. Exp Tech 20(6):27–30
15. Zhang J, Chong TC (1998) Fiber electronic speckle pattern interferometry and its applications in residual stress measurements. Appl Opt 37(27):6707–6715
16. Baldi A (2007a) Full field methods and residual stress analysis in orthotropic material I: linear approach. Int J Solids Struct 44(25–26):8229–8243. doi:10.1016/j.ijsolstr.2007.06.012. http://www.sciencedirect.com/science/article/pii/S0020768307002508
17. Baldi A (2007b) Full field methods and residual stress analysis in orthotropic material II: nonlinear approach. Int J Solids Struct 44(25–26):8244–8258. doi:10.1016/j.ijsolstr.2007.06.002. http://www.sciencedirect.com/science/article/pii/S0020768307002405
18. Ponslet E, Steinzig M (2003) Residual stress measurement using the hole drilling method and laser speckle interferometry part II: analysis technique. Exp Tech 27(4):17–21
19. Schajer G (2010) Advances in hole-drilling residual stress measurements. Exp Mech 50(2):159–168
20. Schajer GS, Steinzig M (2005) Full-field calculation of hole drilling residual stresses from electronic speckle pattern interferometry data. Exp Mech 45(6):526–532
21. Steinzig M, Ponslet E (2003) Residual stress measurement using the hole drilling method and laser speckle interferometry: Part I. Exp Tech 27(3):43–46
22. Gao J, Shang H (2009) Deformation-pattern-based digital image correlation method and its application to residual stress measurement. Appl Optics 48(7):1371–1381
23. Kang KJ, Yao N, He M, Evans A (2003) A method for *in situ* measurement of the residual stress in thin films by using the focused ion beam. Thin Solid Films 443(1):71–77
24. Kang KJ, Darzens S, Choi GS (2004) Effect of geometry and materials on residual stress measurement in thin films by using the focused ion beam. J Eng Mater Technol 126(4):457–464
25. McGinnis M, Pessiki S, Turker H (2005) Application of three-dimensional digital image correlation to the core-drilling method. Exp Mech 45(4):359–367
26. Nelson DV, Makino A, Schmidt T (2006) Residual stress determination using hole drilling and 3D image correlation. Exp Mech 46(1):31–38
27. Sabaté N, Vogel D, Keller J, Gollhardt A, Marcos J, Gràcia I, Cané C, Michel B (2007) Fib-based technique for stress characterization on thin films for reliability purposes. Microelectron Eng 84(5):1783–1787
28. Schajer G, Winiarski B, Withers P (2013) Hole-drilling residual stress measurement with artifact correction using full-field dic. Exp Mech 53(2):255–265
29. Whitehead P, JDL D, Penn D (2008) The application of digital image correlation for measuring residual stress by incremental hole drilling. Appl Mech Mater 13:65–73
30. Schreier HW, Sutton MA (2002) Systematic errors in digital image correlation due to undermatched subset shape functions. Exp Mech 42(3):303–310. doi:10.1007/BF02410987
31. Sun Y, Pang J, Wong C, Su F (2005) Finite element formulation for a digital image correlation method. Appl Opt 44(34):7357–7363
32. Hild F, Roux S (2012) Comparison of local and global approaches to digital image correlation. Exp Mech 52:1503–1519. doi:10.1007/s11340-012-9603-7
33. Roux S, Hild F (2006) Stress intensity factor measurements from digital image correlation: post-processing and integrated approaches. Int J Fract 140(1):141–157
34. Sutton MA, Orteu JJ, Schreier H (2009) Image correlation for shape, motion and deformation measurements: basic concepts, theory and applications. Springer, NY. doi:10.1007/978-0-387-78747-3
35. Del Bimbo A, Nesi P, Sanz J (1995) Analysis of optical flow constraints. IEEE Trans Image Process 4(4):460–469. doi:10.1109/83.370674
36. Horn BKP, Schunck BG (1981) Determining optical flow. Artif Intell 17:185–203
37. Bruhn A, Weickert J, Schnörr C (2005) Lucas/Kanade meets Horn/Schunck: combining local and global optic flow methods. Int J Comput Vision 61(3):211–231
38. Lucas BD, Kanade T (1981) An iterative image registration technique with an application to stereo vision. In: Proceedings of imaging understanding workshop, vol 130, pp 121–130
39. Davis CQ, Freeman DM (1998) Statistics of subpixel registration algorithms based on spatiotemporal gradients or block matching. Opt Eng 37(4):1290–1298
40. Bornert M, Brémand F, Doumalin P, Dupré J, Fazzini M, Grédiac M, Hild F, Mistou S, Molimard J, Orteu J, et al. (2009) Assessment

of digital image correlation measurement errors: methodology and results. Exp Mech 49(3):353–370
41. Wattrisse B, Chrysochoos A, Muracciole J, Nemoz-Gaillard M (2001) Analysis of strain localization during tensile tests by digital image correlation. Exp Mech 41(1):29–39
42. Baldi A, Bertolino F (2013) A posteriori compensation of the systematic error due to polynomial interpolation in digital image correlation. Opt Eng 52:101,913–1–101,913–13. doi:10.1117/1.OE.52.10.101913
43. Valentini E, Benedetti M, Fontanari V, Beghini M, Bertini L, Santus C (2007) Fine increment hole-drilling method for residual stress measurement, proposal of a calibrating apparatus. In: Gdoutos EE (ed) Experimental analysis of nano and engineering materials and structures. Proceedings of the 13th international conference on experimental mechanics, Alexandroupolis, Greece, July 1-6, 2007. Springer, Netherlands, pp 945–946. doi:10.1007/978-1-4020-6239-1_470
44. Leendertz J (1970) Interferometric displacement measurement on scattering surfaces utilizing speckle effect. J Phys E Sci Instrum 3(3):214
45. Timoshenko S, Woinowsky-Krieger S, Woinowsky S (1959) Theory of plates and shells, International edn. McGraw-Hill, New York
46. Pan B, Xie H, Wang Z (2010) Equivalence of digital image correlation criteria for pattern matching. Appl Opt 49(28):5501–5509
47. Baldi A, Bertolino F (2012) Systematic errors due to polynomial interpolation in digital image correlation. analysis of some interpolating kernels and experimental validation. In Speckle 2012: V international conference on speckle metrology. SPIE, Bellingham, WA – USA vol 8413, pp 841,308–1–841,308–6. doi:10.1117/12.97864
48. Schreier HW, Braasch JR, Sutton MA (2000) Systematic errors in digital image correlation caused by intensity interpolation. Opt Eng 39:2915–2921
49. Wang YQ, Sutton MA, Bruck HA, Schreier HW (2009) Quantitative error assessment in pattern matching: effects of intensity pattern noise, interpolation, strain and image contrast on motion measurements. Strain 45(2):160–178
50. Schajer G (1988a) Measurement of non-uniform residual stresses using the hole drilling method: Part I. J Eng Mater Technol 110(4):338–343
51. Schajer G (1988b) Measurement of non-uniform residual stresses using the hole drilling method: Part II. J Eng Mater Technol 110(4):345–349